Appl Phys A (2008) 92: 797–801
DOI 10.1007/s00339-008-4608-x

Applied Physics A
Materials Science & Processing

Thresholds for front-side ablation and rear-side spallation of metal foil irradiated by femtosecond laser pulse

S.I. Anisimov · N.A. Inogamov · Y.V. Petrov · V.A. Khokhlov · V.V. Zhakhovskii · K. Nishihara · M.B. Agranat · S.I. Ashitkov · P.S. Komarov

Received: 12 October 2007 / Accepted: 4 March 2008 / Published online: 28 May 2008

Abstract The mechanical action of laser exposure on a foil may result in the ablation of irradiated front layer and the rear-side spallation. The dynamics of an Al foil is studied by means of two-temperature (2T) hydrodynamics and molecular dynamics (MD). It is found that the rear-side spallation threshold F_s exceeds the front-side ablation threshold F_a. We propose to extend the common approach in laser-matter experiments by pump–probe measuring of the rear-side displacement.

PACS 52.38.Mf · 81.16.-c · 71.15.Pd · 02.70.Ns

The invention of the femtosecond pulse (fsP) lasers belongs to the first-rate achievements of science and technology. The fsP lasers are considered as essential tools for mechanical working on nanoscale. The ultrafast phenomena at nanoscales came to the attention as a skin depth in metals is very small ∼10 nm. The paper describes the dynamics of pressure waves in Al foil simulated by 2T hydrodynamics and MD methods. The strong tensile stress fields during the front-side and rear-side wave reflections are observed in our simulations, as well as the decay of stretched metastable Al through the cavitation in Al melt at the front side of foil (ablation) and the nucleation of cracks in solid Al at the rear side (spallation).

The layer d_T heated by fsP forms for a time t_{eq} shorter than the time $t_s = d_T/c_s$ of sound propagation of d_T, where t_{eq} is an electron-ion thermal relaxation time. Therefore the layer d_T is pressurized by such heating. This fast thermomechanical loading is called as the stress confinement. Therein lies the principal difference between the fast heating by fsP and the slow heating by relatively longer pulses (tens of picoseconds) [1–8]. The dynamics of photomechanical expansion of a Ni film with thickness $d = 50$–100 nm and $d_T \sim 50$ nm is simulated in [1]. Because of ratio $d/d_T \sim 2$ the nucleation zones of ablation and spallation overlap. For this case only ablation threshold F_a exists. As pointed out in [1] F_a grows with increase in d. Our MD simulation with EAM potential [9] reveals that for a larger ratio $d/d_T \sim 7$ the ablation and spallation zones are separated and the distinct thresholds F_a and $F_s > F_a$ exist in either of them.

The slow heating drives a target particle in the line of binodal r–t–b (Fig. 1) and then along the path b–v in two-phase region. It is so because firstly, the pressure created by subsonic heating is relatively small and secondly, the vapor-liquid region in phase diagram is a region of small pressure in contrast with regions of high pressured solid and liquid. Here the points r, t, b, v correspond to the room temperature with $p = 0$, the triple point, a point on binodal, and a point within vapor-liquid region, respectively. The path for the fsP is represented by r–i–b–s–d–v as indicated by Fig. 1, where r–i is an isochoric heating with density ρ_{const}. The point i is an initial point of subsequent unloading. It is far from the binodal, and the pressure p_i is high. According to EOS of Al [10, 11], the pressure on binodal $p_b(T = 2.7\ \text{kK}) = 0.1$ MPa, the pressure in the critical

S.I. Anisimov · N.A. Inogamov (✉) · Y.V. Petrov · V.A. Khokhlov
L.D. Landau Institute for Theoretical Physics RAS, Chernogolovka 142432, Russia
e-mail: nailinogamov@googlemail.com

V.V. Zhakhovskii · K. Nishihara
Institute of Laser Engineering, Yamada-oka 2-6, Suita, Osaka 565-0871, Japan

V.V. Zhakhovskii · M.B. Agranat · S.I. Ashitkov · P.S. Komarov
Joint Institute of High Temperature RAS, 13/19 Izhorskaya street, Moscow 125412, Russia

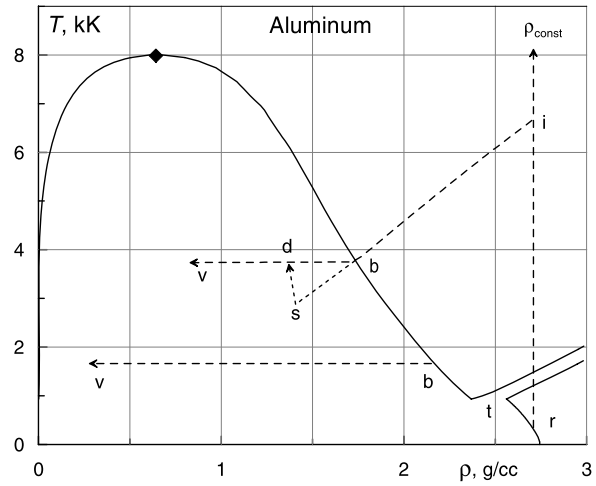

Fig. 1 Phase path r–i–b–s–d–v of an Al particle of target irradiated by fsP. Phase diagram taken from [10]

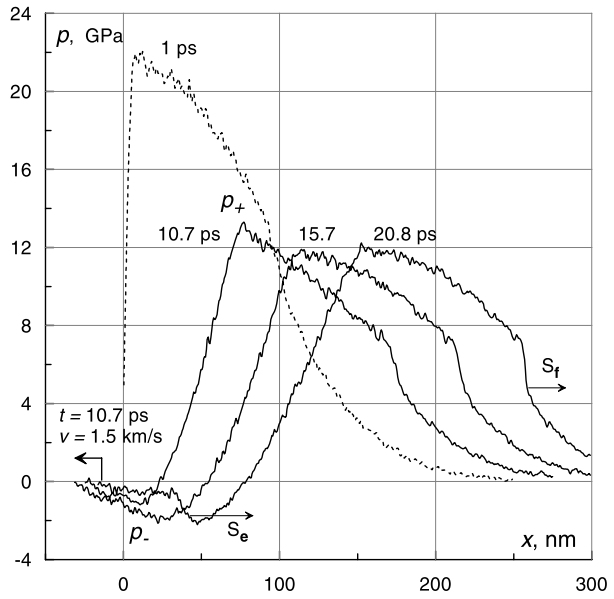

Fig. 2 The process of acoustic decay. The initial pressure $p(x, t = 1\ \text{ps})$, and formation of quasi-steady twofold pulse with two shocks S_e and S_f

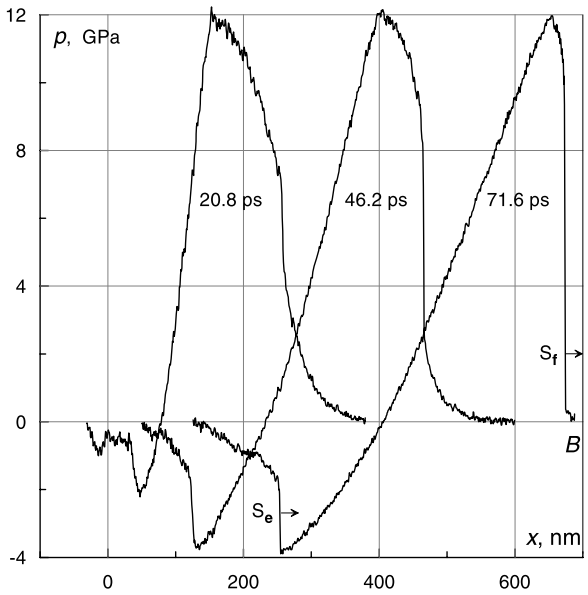

Fig. 3 The end of acoustic decay: the twofold pulse moves from the front boundary. In continuation of Fig. 2

point $p_c = 0.3$–0.6 GPa, and the pressure in the point i is $p_i(\rho = 2.7\ \text{g/cc}, T = 2.7\ \text{kK}) = 15$ GPa.

The fsP leads to evaporation of target layer h_{ev}. Hertz formula gives $h_{ev} \sim \tau\sqrt{T/2\pi m}\rho_v/\rho_l$, where ρ_v and ρ_l are densities of vapor and liquid, τ is an evaporation duration. By taking the saturated vapor density at surface temperature 1–2 kK and the characteristic cooling time for metals $\tau \sim 0.1$–1 ns as an evaporation duration, one can obtain $h_{ev} \ll 1$ nm for fluence $F < F_a$ from Hertz formula. The fsP above the ablation threshold F_a ablates a target by mechanical breaking in range of 10 to ~100 nm.

In an early stage of ablation the Gaussian curve can be used as a given initial temperature profile for MD simulation, see details in [12]. The temperature is adjusted by heating up Al atoms during 1–2 ps with using the Langevin thermostat. The dotted line in Fig. 2 is a pressure profile corresponding to the initial temperature $T_0(x) = 4.7\exp(-x^2/d_T^2) + 0.3$ kK, where $T_0(0) = 5$ kK is a surface temperature. The function $T_0(x)$ and the heated depth d_T are defined from the 2T hydrodynamical model [1, 2, 4, 5, 12–14], which yields $d_T \approx 110$ nm for Al in the range of absorbed fluence $F = 0.07$–$0.2\ \text{J/cm}^2$.

"Supersonic" formation of pressurized region near the vacuum boundary (initially located in $x = 0$ on Fig. 2) has two important mechanical effects. First, a matter begins to move towards vacuum as a result of propagation of the rarefaction wave $p_- p_+$ situated to the left of maximum p_+ on the pressure profiles in Fig. 2. This wave causes the thermomechanical ablation at the front side. Second, the compression wave propagates to the right and causes spallation of target on rear side nearby the right vacuum boundary B shown in Fig. 3. The initial pressure (dotted line in Fig. 2) transforms to the steady twofold wave (see $t = 71.6$ ps in Fig. 3). In linear acoustics the initial pressure profile can be decomposed in the two waves, which is why the pressure drops by half.

As mentioned in [12], the twofold wave consists of the compression $p > 0$ and the stretching $p < 0$ zones, see also [1, 2, 4, 5]. The focusing of characteristics results in the breaking of compression wave with formation of a leading shock S_f shown in Figs. 2, 3. The shock S_e on the trailing front of twofold wave appears due to the cavitation rupture of Al melt. Shocks S_e, S_f are the left and right ends of the

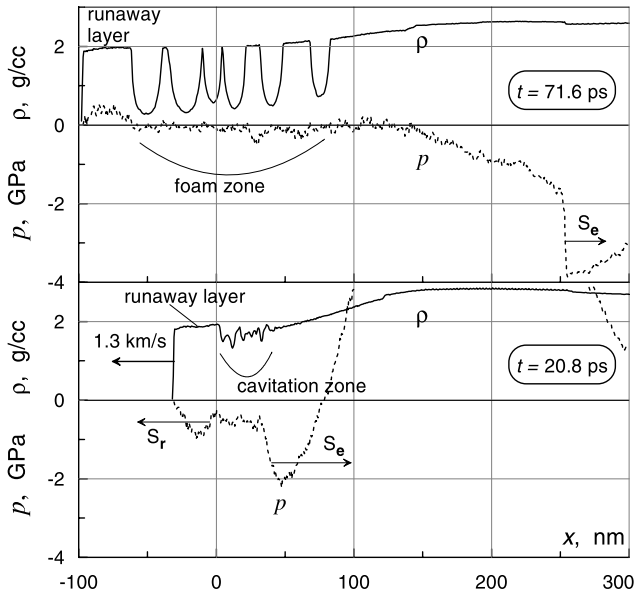

Fig. 4 Formation of a runaway layer on the left end of cavitation zone at 20.8 ps, and detachment of the runaway layer associated with decay of dynamically weak foam at 71.6 ps

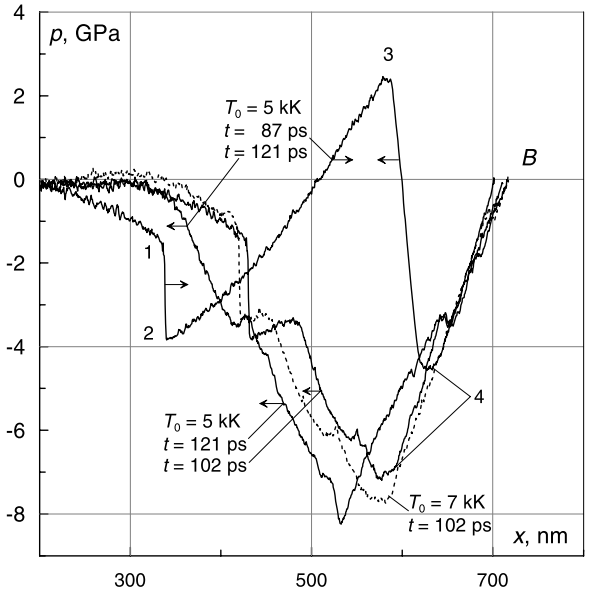

Fig. 5 Reflection of twofold pulse from the rear side B

rarefaction wave moving rightwards with local sound speed. The shock S_f is supersonic relative to the medium on its right and subsonic relative to the medium on its left, so the rarefaction wave catches up S_f thus depressing it. In a similar manner the shock S_e moving with supersonic speed (but slower than S_f) through stretched material catches up the rarefaction wave. The S_e reduces the tensile stress to zero. The amplitudes of both shocks slowly decrease in time. Figure 3 demonstrates formation and propagation of this quasi-steady twofold pulse. The shape of twofold pulse is changed slowly due to the small at $F \sim F_a$ sound velocity dispersion. Therefore the obtained simulation results on the rear-side spallation for a foil 0.7 μm thick will be valid for thicknesses from 0.4 μm to ∼2 μm.

The pressure valley p_-, $p < 0$ becomes deeper with time due to propagation of the wave reflected from the left boundary, as evident from the positions of minima at the profiles $t = 10.7$ ps and $t = 15.7$ ps in Fig. 2. Bubble nucleation starts from 17 ps when the stress reaches 2 GPa. From that time a great number of bubbles appears within the next few picoseconds. The distances between them are small with respect to the transverse dimensions l_y, l_z of MD-box. The pressure in the cavitation zone grows up to zero in a few picoseconds since the stretching stress is released as indicated in Fig. 4 for $t = 20.8$ ps. As a result the runaway layer separates from the target and two shocks S_e, S_r move from the cavitation zone.

Reflection of twofold pulse from the rear side B is shown in Fig. 5. The pressure profile consists of 1-2-3 and 3-4-B parts. The 1-2-3 is a residual of twofold pulse. It includes the shock S_e denoted as 1-2 and a residual of rarefaction wave $p_- p_+$. The 3-4-B is a sum of twofold pulse and its reflection. The leading front of reflection wave lies in point 3. After reflection the shock S_f transforms into the rarefaction wave 3-4, whereas the rarefaction wave $p_- p_+$ becomes the compression wave 4-B. In time, the twofold pulse residual 1-2-3 moves rightwards and decreases in length, cf. profiles for 87 ps and 102 ps in Fig. 5. The stretching stress reaches the maximum 8 GPa when two minima 2 and 4 meet at 121 ps. In linear acoustics the maximum stress 16 GPa is equal to a sum of amplitudes of shocks S_e and S_f.

The maximum stretching stress 8 GPa is equal to one-half of 16 GPa derived from the linear acoustics. The difference results mainly from nonlinearity caused by the strong plastic effects near the spallation threshold F_s. Pressure profiles for $T_0 = 5$ kK in Fig. 5 correspond to the absorbed fluence below the threshold F_s, whereas the profile for $T_0 = 7$ kK represents simulation above the threshold. F_s is achieved for the initial front temperature $T_0(0) \approx 6$ kK. Below the threshold the stretching stress decreases with time since the stretching deformation reaches its maximum. After a time, the expanding quiet zone arises near point B.

For $F \approx F_s$ the rear-side spallation starts near $-p_s$ as illustrated by Figs. 5, 6. Time evolution of density maps (Fig. 6) indicates that the rupture of solid results from formation of cracks. On acoustic time scale the disruption is a fast process. As a result the stretching stress rapidly drops to zero in the region of crack formation as shown by spike in Fig. 6. The spalled layer has a thickness $h_s \approx 170$ nm, which is determined by d_T as $h_s \propto d_T$, and it depends weakly on the foil thickness if it is less than 2 μm. For a thicker foil the sound dispersion of twofold pulse should be taken into account. This causes h_s to increase directly with the foil thickness [4, 7].

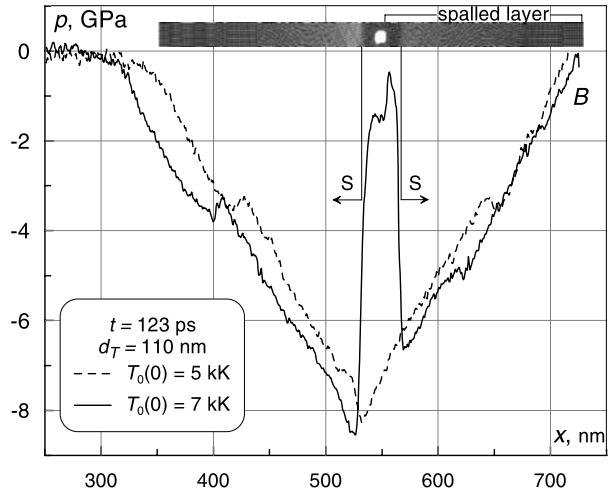

Fig. 6 Pressures for the rear-side spallation below threshold ($T_0 = 5$ kK), and above threshold ($T_0 = 7$ kK) with density map for $T_0 = 7$ kK. The profiles are similar except the zone around the rupture where pressure spike grows fast

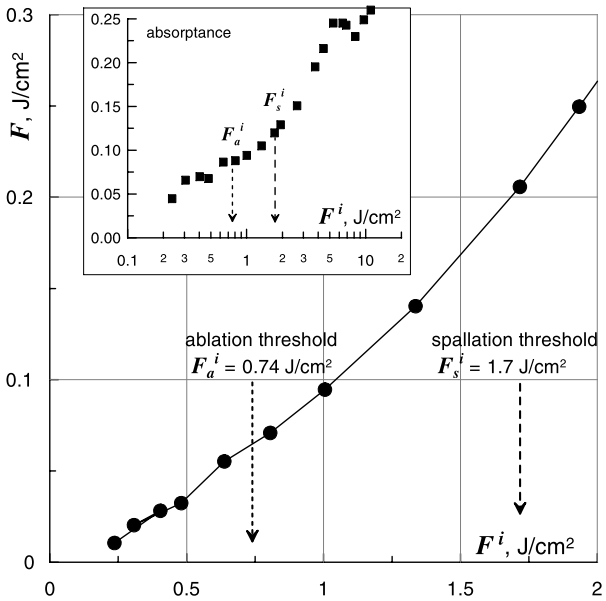

Fig. 7 Ablation and spallation thresholds, and the experimental absorptance $A(F^i)$ and absorbed fluence $F(F^i)$

MD simulations give the threshold temperatures $T_0(0) = 2.6$ kK [12] for the front-side ablation and 6 kK for the rear-side spallation. The ablation threshold is $F_a = 0.07$ J/cm^2 [12]. The small part of this energy $E_k(F) \approx 0.005$ J/cm^2 is spent for acceleration of material at the 2T stage of motion. The kinetic energy $E_k(F)$ increases with fluence increase: $E_k(0.12) \approx 0.015$ J/cm^2, and $E_k(0.2) \approx 0.05$ J/cm^2. Combining 2T and MD data for T_0, d_T and E_k we obtain $F_s \approx 0.2$ J/cm^2 for the rear-side spallation threshold.

The incident fluence threshold F_s^i for a fixed threshold F_s depends on the polarization and the incident angle of a laser beam, whereas F_s is a characteristic of substance. F_s does not depend on polarization, inclination, and even on light wavelength, if the pulse duration is shorter 1 ps. The experimental absorptance $a(F^i) = F/F^i$, and $F(F^i) = F^i a(F^i)$ for the pump pulse in our femtosecond chromium-forsterite laser system [12, 13] are shown in Fig. 7. Using $F(F^i)$ and $F_s \approx 0.2$ J/cm^2 we evaluate $F_s^i \approx 1.7$ J/cm^2.

The one-dimensional approach used above is appropriate for description of rear-side spallation if the foil thickness is much smaller than diameter of a pump spot ~50 μm. When the difference $F - F_s$ increases the thickness of the spalled layer h_s decreases, while its velocity increases. The pump pulse has a Gaussian distribution of fluence $F(r)$ over the laser spot with a maximum in the spot center $r = 0$. Therefore there are an ablation cupola and a crater with abrupt boundary at a radius r_c where local fluence $F(r_c)$ equals F_a [8]. These morphological features are observed on the front side of target in the pump–probe experiments with Newton rings and with microinterferometric measurements. The similar spalled cupola and the crater arise on the rear side. It is proposed to supplement observations of Newton rings and microinterferometric fringes at the front side with the analogous experiments on the rear side of target. The probe beam can be send to both surfaces of a foil to measure displacements of front and rear surfaces as functions of time and radius.

The physics of spallation has received much attention [11]. There are a variety of devices such as explosives, ion beams, lasers, which differ in the length l and the deformation rate $\dot{V}/V$ of the samples under investigation ($\dot{V}/V \sim v/l$ where v is expansion velocity). An important part of these devices is the VISAR system, which measures the rear-side velocity of a foil. As noted above, the pump–probe laser system can operate as a VISAR system, providing a means to measure nanoscale displacements. Such experiments will allow to obtain information about the tensile strength of condensed matter at extremely high rates $\dot{V}/V$.

1 Conclusion

The paper contains description of nonlinear acoustic effects connected with sonic dispersion which leads to the breaking of compression wave and formation of the shock S_f, see Figs. 2 and 3. MD simulations of laser-matter interaction done in previous works were performed with number of atom less than a million while 76 million Al atoms are simulated in our work. This enabled us to observe the process of steepening of pressure gradient during focusing of characteristics in a long MD box with large cross section [12]. It appears that the fsP can be used as a very fine driver of rear-side spallation. For the first time we find the formation of shock S_e at $p < 0$ due to release of stretching stress when

nucleation begins for $F > F_a$. Therefore it is possible to investigate continuation of Hugoniot adiabat across the binodal into $p < 0$ region in future studies.

Acknowledgements The work is supported by RFBR grant No. 07-02-00764.

References

1. E. Leveugle et al., Appl. Phys. A **79**, 1643 (2004)
2. A.N. Volkov et al., J. Phys. Conf. Ser. **59**, 640 (2007)
3. P. Lorazo et al., Phys. Rev. B **73**, 134108 (2006)
4. F. Vidal et al., Phys. Rev. B **70**, 184125 (2004)
5. J.P. Colombier et al., Phys. Rev. B **71**, 165406 (2005)
6. V.V. Zhakhovskii et al., JETP Lett. **71**, 167 (2000)
7. H. Tamura et al., J. Appl. Phys. **89**, 3520 (2001)
8. S.I. Anisimov et al., JETP **103**, 183 (2006)
9. Y. Mishin et al., Phys. Rev. B **59**, 3393 (1999)
10. A.V. Bushman et al., *Intense Dynamic Loading of Condensed Matter* (Taylor & Francis Transl., 1993), p. 295
11. G.I. Kanel, S.V. Razorenov, V.E. Fortov, in *Shock-Wave Phenomena and the Properties of Condensed Matter*, ed. by L. Davidson, Y. Horie. High-Pressure Shock Compression of Condensed Matter (Springer, Berlin, 2004)
12. S.I. Anisimov et al., The article 278 for the COLA-2007
13. M.B. Agranat et al., JETP Lett. **85**(6), 271 (2007)
14. K. Eidmann et al., Phys. Rev. E **62**, 1202 (2000)